

Radiologic and Histologic Correlates of Early Interstitial Lung Changes in Explanted Lungs


Stijn E. Verleden, PhD • Arno Vanstapel, MD, PhD • Joseph Jacob, MD, PhD • Tinne Goos, MD • Jeroen Hendriks, MD, PhD • Laurens J. Ceulemans, MD, PhD • Dirk E. Van Raemdonck, MD, PhD • Laurens De Sadeleer, MD, PhD • Robin Vos, MD, PhD • Johanna M. Kwakkel-van Erp, MD, PhD • Arne P. Neyrinck, MD, PhD • Geert M. Verleden, MD, PhD • Matthieu N. Boone, PhD • Wim Janssens, MD, PhD • Els Wauters, MD, PhD • Birgit Weynand, MD, PhD • Danny D. Jonigk, MD, PhD • Johnny Verschakelen, MD, PhD • Wim A. Wuyts, MD, PhD

From the Department of Chronic Diseases and Metabolism, BREATHE (S.E.V., A.V., T.G., L.J.C., D.E.V.R., L.D.S., R.V., G.M.V., W.J., E.W., W.A.W.), Department of Cardiovascular Sciences (A.P.N.), and Department of Imaging and Pathology (B.W., J.V.), KU Leuven, Herestraat 49, 3000 Leuven, Belgium; Department of ASTARC, University of Antwerp, Antwerp, Belgium (S.E.V., J.H.); Department of Respiratory Medicine (S.E.V., J.M.K.v.E.) and Department of Thoracic and Vascular Surgery (S.E.V., J.H.), University Hospital Antwerp, Antwerp, Belgium; Department of Respiratory Medicine (J.J.) and Centre for Medical Image Computing (J.J.), University College London, London, UK; Department of Thoracic Surgery, University Hospital Leuven, Leuven, Belgium (L.J.C., D.E.V.R.); Department of Physics and Astronomy, Ghent University, Ghent, Belgium (M.N.B.); Institute of Pathology, Hannover Medical School, Hannover, Germany (D.D.J.); and Biomedical Research in Endstage and Obstructive Lung Disease Hannover (BREATHE), Member of the German Center for Lung Research (DZL), Hannover, Germany (D.D.J.). Received May 9, 2022; revision requested July 6; revision received October 13; accepted November 4. **Address correspondence to** W.A.W. (email: wim.wuyts@uzleuven.be).

This research was funded in whole, or in part, by the Wellcome Trust (209553/Z/17/2). A.V. is supported by a fundamental research grant from the Research Foundation Flanders (FWO; 1102020N). T.G. is supported by a strategic research grant from the FWO. R.V. is a senior clinical research fellow of the FWO. J.J. was supported by the National Institutes of Health Research at the University College London Hospitals Biomedical Research Centre. The Ghent University Centre for X-ray Tomography is supported by Bijzonder Onderzoeksfonds UGent (BOF.EXP.2017.0007). D.D.J. is supported by a grant from the European Research Council (XHALE). E.W. is supported by Stichting Tegen Kanker (Mandate for basic & clinical oncology research). W.A.W. is supported by a senior clinical investigator grant from the FWO (1832522N).

Conflicts of interest are listed at the end of this article.

See also the editorial by Jedy in this issue.

Radiology 2023; 307(1):e221145 • <https://doi.org/10.1148/radiol.221145> • Content codes: 

Background: Interstitial lung abnormalities (ILAs) reflect imaging features on lung CT scans that are compatible with (early) interstitial lung disease. Despite accumulating evidence regarding the incidence, risk factors, and prognosis of ILAs, the histopathologic correlates of ILAs remain elusive.

Purpose: To determine the correlation between radiologic and histopathologic findings in CT-defined ILAs in human lung explants.

Materials and Methods: Explanted lungs or lobes from participants with radiologically documented ILAs were prospectively collected from 2010 to 2021. These specimens were air-inflated, frozen, and scanned with CT and micro-CT (spatial resolution of 0.7 mm and 90 μ m, respectively). Subsequently, the lungs were cut and sampled with core biopsies. At least five samples per lung underwent micro-CT and subsequent histopathologic assessment with semiquantitative remodeling scorings. Based on area-specific radiologic scoring, the association between radiologic and histopathologic findings was assessed.

Results: Eight lung explants from six donors (median age at explantation, 71 years [range, 60–83 years]; four men) were included (unused donor lungs, $n = 4$; pre-emptive lobectomy for oncologic indications, $n = 2$). Ex vivo CT demonstrated ground-glass opacification, reticulation, and bronchiectasis. Micro-CT and histopathologic examination demonstrated that lung abnormalities were frequently paraseptal and associated with fibrosis and lymphocytic inflammation. The histopathologic results showed varying degrees of fibrosis in areas that appeared normal on CT scans. Regions of reticulation on CT scans generally had greater fibrosis at histopathologic analysis. Vasculopathy and bronchiectasis were also often present at histopathologic examination of lungs with ILAs. Fully developed fibroblastic foci were rarely observed.

Conclusion: This study demonstrated direct histologic correlates of CT-defined interstitial lung abnormalities.

© RSNA, 2022

Supplemental material is available for this article.

Interstitial lung abnormalities (ILAs) refer to specific CT findings potentially compatible with interstitial lung disease (ILD) in patients where morphologic disease at CT imaging was not expected (1). A recent position paper by the Fleischner Society put forward a more uniform description of ILAs as ground-glass or reticular abnormalities, lung distortion, traction bronchiectasis, honeycombing, and nonemphysematous cysts encompassing at least 5% of any lung zone. The importance of ILAs has been demonstrated in several population-based and lung cancer screening studies. For individuals older than 60 years, the

incidence of ILAs is estimated to be 4%–9% in those who smoke and 2%–7% in those who do not (2). Importantly, ILAs—mostly those with a subpleural distribution—are associated with subsequent progression to true ILD and higher mortality. According to the current literature, up to 20% of ILAs progress within 2 years, while over 40% progress within 5 years (2).

While knowledge of the incidence, risk factors, and prognosis of ILAs has markedly improved recently (1,2), the exact morphologic and histopathologic correlates of these imaging features remain elusive. Miller et al (3)

Abbreviations

ILA = interstitial lung abnormality, ILD = interstitial lung disease, IPF = idiopathic pulmonary fibrosis

Summary

The histopathologic features of interstitial lung abnormalities included paraseptal organized fibrosis and lymphocytic inflammation that were present in regions considered normal at CT.

Key Results

- In eight explanted lungs or lobes with interstitial lung abnormalities (ILAs) from six donors, histopathologic analysis showed varying degrees of fibrosis in areas that appeared normal at CT.
- Fibrosis in lungs with ILAs was organized paraseptally and was associated with predominant lymphocytic inflammation.
- Vasculopathy and bronchiectasis were also often present at histopathologic examination of lungs with ILAs, while fully developed fibroblastic foci were only rarely observed.

found ILAs in 26 of 424 (6%) tumor resection specimens, of which three (12%) demonstrated a centrilobular distribution, 17 (65%) were subpleural, and six (23%) were of mixed distribution. Hung et al (4) analyzed 397 lung tumor resection specimens where 101 (25%) patients showed parenchymal abnormalities. Of the 397 specimens, 41 (10%) were classified as having fibrotic remodeling and mostly corresponded to smoking-related interstitial fibrosis. The presence of histopathologic abnormalities also correlated with the presence of ILAs at CT imaging. To our knowledge, no studies have specifically investigated the correlation between ILA patterns on CT scans and histologic findings.

A protocol to perform accurate matching of in vivo CT scans with histologic findings using ex vivo CT and micro-CT imaging as intermediate steps has been developed (5–8). In idiopathic pulmonary fibrosis (IPF), the inherent spatial heterogeneity associated with usual interstitial pneumonia, the typical radiologic pattern observed in IPF, was exploited to compare areas of minimal and fully developed fibrosis. Interestingly, fibrosis and cyst formation manifested at the periphery of the pulmonary lobule and progressively extended toward the core of this anatomic compartment (9). A major limitation of these previous studies was that all lungs had end-stage disease, and it remains unknown whether these changes are observed at the early stages. Therefore, the purpose of this study was to investigate the correlations between radiologic and histopathologic findings in whole lungs or lobes with CT-defined ILAs.

Materials and Methods**Study Participants and Data**

In this prospective institutional review board (IRB)–approved study, all participants who underwent pre-emptive lobectomy provided written informed consent. Unused donor lungs deemed to be of insufficient quality for transplant were collected from 2010 to 2021 (IRB S52174, S61653). For most of these specimens, in vivo CT scans were unavailable. Lobar specimens following tumor resection in cases where the suspicious nodule was initially wedge-resected and found to be

malignant were also collected in 2020 (IRB S63093). Unused donor lungs and lobar lung resection specimens were also collected from a second site in 2021 (IRB B3002021000073).

CT and Micro-CT Acquisition

Collected lungs or lobes were air-inflated at 30-cm water pressure and frozen in liquid nitrogen following gentle deflation to 10-cm water pressure. An ex vivo CT scan was then obtained with a SOMATOM (Siemens) or Revolution CT (GE Healthcare) scanner (tube voltage, 120 kVp; tube current, 10 mA; field of view, 300 mm; collimation, 0.6 mm; section thickness, 1-mm with an increment of 0.7 mm). Following ex vivo CT, whole-lung micro-CT was performed with either a HECTOR (Ghent University [10]) or UniTOM XL (TESCAN [22]) scanner (tube voltage, 80 kVp; tube current, 0.300 mA; field of view, 257 mm; voxel size, 0.09 mm) with the lung in a frozen state to improve the accuracy of matching between ex vivo CT and specimen micro-CT scans. Subsequently, the lungs were sliced with a bandsaw at a 2-cm slice thickness, and cores with a diameter of 14–20 mm were systematically extracted from these samples. A photograph was taken before and after the samples were removed to ensure accurate matching between in vivo CT (if available), ex vivo CT, whole-lung micro-CT, and core micro-CT and histologic staining. Micro-CT was performed at –30°C (Skyscan 1272; Bruker [voxel size, 10 µm; rotation step, 0.5]). Cores were selected to represent the spatial heterogeneity in the lung in areas surrounding the CT-identified ILAs, ranging from no visible abnormalities to obvious opacities visible on ex vivo CT scans. Five areas per lung were analyzed, except for one case where six areas were investigated because there was more spatial heterogeneity of disease. These samples subsequently underwent fixation with 6% paraformaldehyde and were dehydrated and paraffin-embedded. The study design and workflow are further illustrated in Figure 1.

CT and Micro-CT Assessment

The ex vivo CT scan was assessed by two experienced thoracic radiologists (J.J., with 15 years of CT experience, and J.V., with 34 years of CT experience) who were blinded to all participant information, and a systematic description of the general radiologic pattern (reticulation, ground-glass opacification, honeycombing, and bronchiectasis) and overall extent of parenchymal remodeling was provided. The spatial heterogeneity of disease in areas on ex vivo CT scans from which the cores were later taken was assessed by the same two thoracic radiologists, one as the main observer and one to assess consistency of the scoring. The degree of normal tissue, reticulation, and ground-glass opacification were assessed per individual lung core using a semiquantitative scale (0%–100%, estimated to the nearest 5%), while the degree of bronchiectasis was assessed as either present or absent. Micro-CT–based segmentation of selected airways was performed using ITK-SNAP (<http://www.itksnap.org/>).

Histopathologic Assessment

Histologic slices were cut and stained with hematoxylin-eosin, trichrome, and Van Gieson stain. All slices were inves-

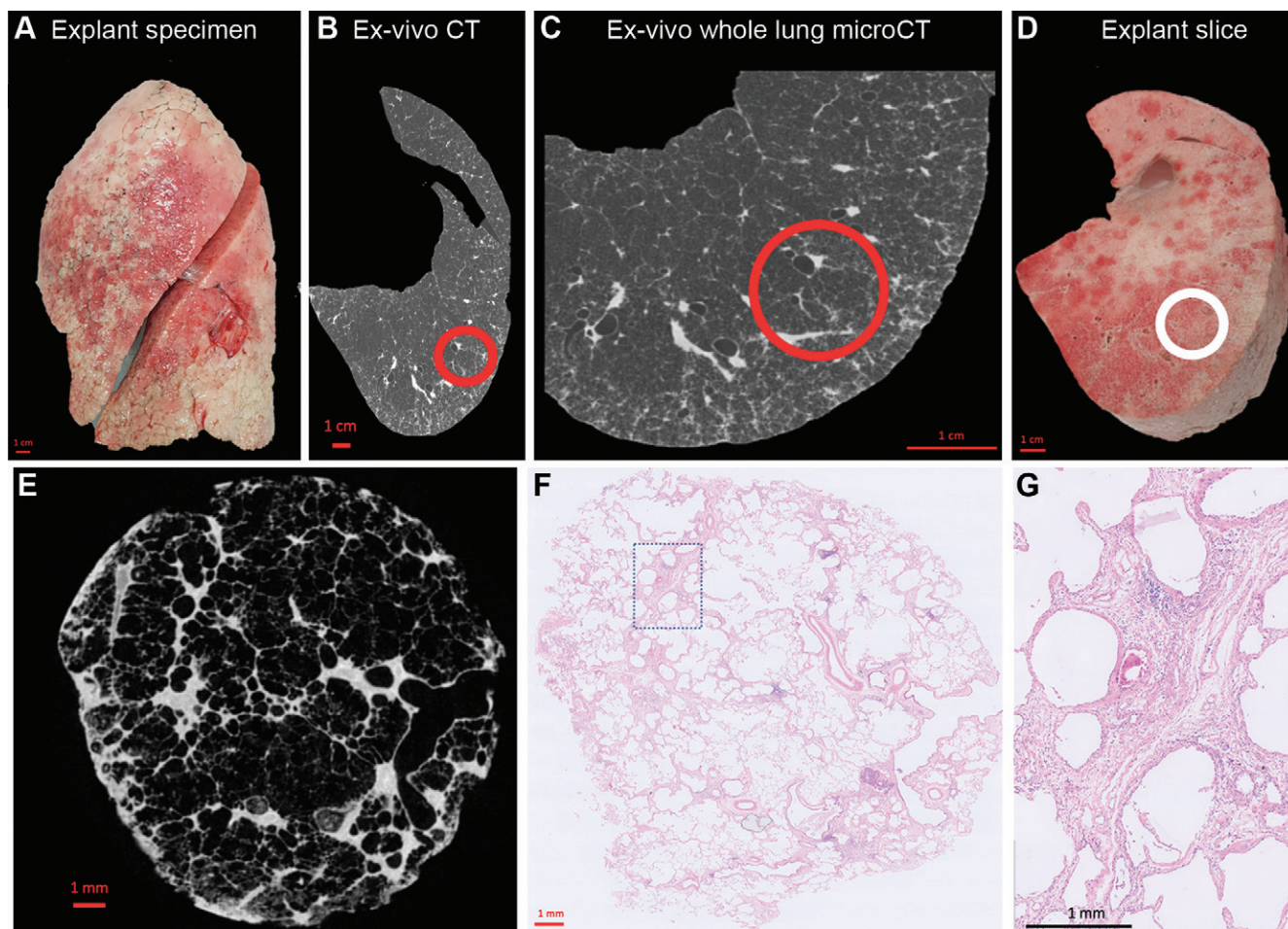


Figure 1: Study design. **(A)** Photograph shows the explanted lung frozen solid in liquid nitrogen fumes. **(B)** Axial noncontrast ex vivo CT scan of the specimen is obtained while it is frozen. **(C)** Whole-lung micro-CT scan is obtained for better spatial resolution. **(D)** Photograph shows the lung sliced transversally in 2-cm slices. **(E)** Micro-CT scan of a core sample (indicated with the circle in **B–D**) is obtained. **(F)** Matched histologic image (hematoxylin-eosin stain; magnification, $\times 5$) is shown at the same location as the micro-CT scan. **(G)** High-magnification histologic image (hematoxylin-eosin stain; magnification, $\times 20$) shows paraseptal fibrosis.

tigated by a pulmonary pathologist (D.D.J., with 16 years of experience in nonneoplastic lung pathology), who was blinded to clinical information, and assessed for the following parameters: (*a*) presence, location (paraseptal, peribronchial, and interstitial), and severity and/or amount of fibrosis (0, no evidence of fibrosis; 1, mild fibrosis with no clear organization of fibrosis observed; 2, moderate fibrosis with beginning organization of fibrosis; 3, severe fibrosis as seen in end-stage lung disease); (*b*) presence of vasculopathy (ie, abnormalities in the vasculature, such as intimal thickening; yes or no); (*c*) presence of fibroblastic foci (yes or no; if yes, fully developed or incomplete); (*d*) location (paraseptal, peribronchial, and interstitial) and type of predominant inflammation (indicated by neutrophils, lymphocytes, or macrophages); (*e*) presence of bronchiectasis; and (*f*) other potentially relevant findings.

Statistical Analysis

Results are expressed as either means or medians. Variables were dichotomized based on the predominant local CT pattern ($\geq 70\%$ healthy, $\geq 50\%$ reticulation, $\geq 40\%$ ground-glass opacification vs lower percentages) and compared using the Mann-Whitney *U* test. $P < .05$ was considered indicative of a

statistically significant difference. All analyses were performed using Prism version 9.0 (GraphPad).

Results

Study Participants and Data

A total of 103 unused donor lungs or lobes from 84 participants were collected since 2010. The ex vivo lung CT scan was assessed and six lungs of four participants showed evidence of ILAs on the scan, while the medical history did not reveal any known pulmonary disease prior to organ donation. Five lobes from tumor resection surgery were collected since 2020, of which two showed signs of ILAs in participants who were not known to have chronic lung disease and where an incidental nodule was found. Due to technical limitations, in one lung of the included lung pairs derived from an unused donor, ex vivo CT analysis alone was undertaken with no histopathologic analysis performed. The flowchart is shown in Figure 2. Our study included eight explanted specimens from a total of six participants (unused donor lungs, $n = 6$ from four participants; tumor resection specimens, $n = 2$ from two participants). The median age at

explanation was 71 years (range, 60–83 years) and four donors were men. Participant characteristics are summarized in Table 1.

Radiologic Assessment

A varying degree of subpleural ground-glass opacification and reticulation was found in all lungs, as confirmed by both observers (Fig S1). Patterns compatible with lung damage were more pronounced in the lower lobes in five of the eight specimens (four participants; Fig S1A, S1C, S1D, S1G, S1H), while the opacities did not show a basal predominance in the other three specimens (two participants; Fig S1B, S1E, S1F). Two specimens were only mildly affected (5%–10% of lung volume; Fig S1A, S1H), four were moderately affected (10%–20% of lung volume; Fig S1B, S1C, S1D, S1G), and two specimens were severely affected (20%–30% of lung volume; Fig S1E, S1F). Besides ground-glass opacification and reticulation, five specimens showed evidence of bronchiectasis (all specimens according to the second radiologist), and two had some degree of emphysema as characterized by the presence of subpleural bullae or paraseptal emphysema (Table 1).

Histopathologic Assessment

A total of 36 samples from seven specimens were separately assessed based on the ex vivo CT scan and showed median values of 40% (range, 25%–75%), 25% (range, 15%–40%), and 20% (range, 10%–30%) for normal tissue, reticulation, and ground-glass opacification, respectively. The main findings are summarized in Table 2, with representative examples shown in Figure 3.

Of the 36 samples, 30 (83%) showed some degree of fibrosis at histopathologic assessment (mild, *n* = 20; moderate, *n* = 10). This was organized exclusively peribronchial in two of 36 (6%) samples and exclusively paraseptal in six of 36 (17%) samples, but never exclusively interstitial. A combination of paraseptal and interstitial changes was observed in nine of 36 (25%) samples, and a combination of peribronchial and paraseptal changes was observed in three of 36 (8%) samples. In 10 of 36 (28%) samples, fibrosis was present in all compartments (peribronchial, paraseptal, and interstitial). Taken together, paraseptal fibrosis was the most frequent distribution observed in 28 of 36 (78%) samples, followed by interstitial fibrosis in 19 of 36 (53%) samples and peribronchial fibrosis in 15 of 36 (42%) samples. Among the 36 samples, fully developed fibroblastic foci were present in only three samples (8%)

of three different lungs (three participants), with incomplete fibroblastic foci in an additional four samples (11%). These foci were exclusively found in association with fibrosis (mild, *n* = 5; moderate, *n* = 2) and in areas with lymphocytic inflammation. Interestingly, vasculopathy was present in six of the seven samples with fibroblastic foci.

Inflammation was present in 31 of 36 (86%) samples and was almost exclusively dominated by lymphocytes (peribronchial, *n* = 2; paraseptal, *n* = 5; interstitial, *n* = 7; peribronchial and paraseptal, *n* = 2; paraseptal

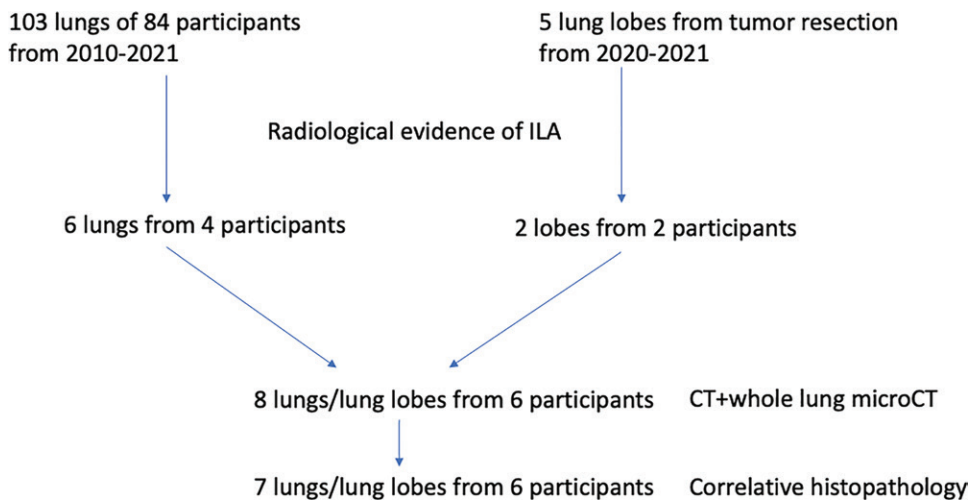


Figure 2: Flowchart of participant inclusion. ILA = interstitial lung abnormality.

Table 1: Participant Characteristics and Radiologic Scoring

Age (y)/Sex	Smoking Status	Source of Tissue	Extent of Disease	Localization	Reticulation	GGO	BRECT	Emphysema
60/M	Unknown	Unused donor R	10%–20%	Lower lobe	x	x	x	
60/M	Unknown	Unused donor L	5%–10%	Lower lobe	x	x		
65/F	30 pack-years	Tumor resection LLL	10%–20%	Lower lobe	x	x		
69/M	Unknown	Unused donor L	10%–20%	Lower lobe	x	x	x	x
70/M	Never smoker	Unused donor R	5%–10%	Diffuse	x	x	x	x
76/M	20 pack-years	Tumor resection RLL	10%–20%	Lower lobe	x	x	x	
83/F	Never smoker	Unused donor R	20%–30%	Diffuse	x	x		
83/F	Never smoker	Unused donor L	20%–30%	Diffuse	x	x	x	

Note.—Six unused donor lungs from four participants and two tumor resection specimens from two participants were included. The extent of disease is indicated by the percentage of affected lung volume. BRECT = bronchiectasis, GGO = ground-glass opacification, L = left, LLL = left lower lobe, R = right; RLL = right lower lobe.

Table 2: Main Histologic Findings of Lung Samples with Interstitial Lung Abnormalities

Histologic Feature	Value (<i>n</i> = 36)
Fibrosis	30 (83)
Peribronchial	2 (6)
Interstitial	0 (0)
Paraseptal	6 (17)
Peribronchial and paraseptal	3 (8)
Paraseptal and interstitial	9 (25)
All compartments	10 (28)
Lymphocytic inflammation	31 (86)
Peribronchial	2 (6)
Interstitial	7 (19)
Paraseptal	5 (14)
Peribronchial and paraseptal	2 (6)
Paraseptal and interstitial	10 (28)
All compartments	5 (14)
Vasculopathy	12 (33)
Bronchiectasis	14 (39)
Fibroblastic foci	
Fully developed	3 (8)
Incomplete	4 (11)

Note.—Data are numbers of samples, with percentages in parentheses. A total of 36 samples from seven lungs were included for further histologic assessment.

and interstitial, *n* = 10; and peribronchial, paraseptal, and interstitial, *n* = 5).

Lymphocytic inflammation was present in four of six (67%) samples without fibrosis, in 17 of 20 (85%) samples with mild fibrosis, and in all 10 samples (100%) with moderate fibrosis. Neutrophilic inflammation was not observed, while one sample showed a desquamative interstitial pneumonia characterized by macrophage inflammation.

Vasculopathy was present in four lungs of three participants; three of six (50%) samples were without concomitant fibrosis, five of 20 (25%) samples had mild fibrosis, and four of 10 (40%) samples had moderate fibrosis.

Histopathologic evidence of bronchiectasis was observed in 14 of 36 (39%) samples and was present in six of the seven studied lungs (five participants) (Table S1). Bronchiectasis was found in areas without histopathologic evidence of fibrosis (17% [one of six] of samples without fibrosis), areas with mild fibrosis (45% [nine of 20] of samples with mild fibrosis), and in areas with moderate fibrosis (40% [four of 10] of samples with moderate fibrosis). An example of airway distortion in the peripheral preterminal airways, observed in the absence of severe interstitial fibrosis, in lungs with ILAs is shown in Figure 4.

Radiologic and Histopathologic Correlation

Core-specific information concerning radiologic and histopathologic findings is detailed in Table S1. There was 80%, 86%, and 80% consistency in the assessment of healthy tissue, reticulation, and ground-glass opacification, respectively, between the two radiologist observers. Regions that showed

limited evidence of remodeling based on radiologic scoring of ex vivo CT scans ($\geq 70\%$ core volume of healthy parenchyma, 11 of 36) nevertheless contained considerable fibrosis at histopathologic analysis (mild fibrosis, *n* = 8), indicating that the degree of fibrosis in relatively normal appearing lung was underestimated with CT (organization: paraseptal, *n* = 7; interstitial, *n* = 5; peribronchial, *n* = 4). A representative example is shown in Figure S2. This was also accompanied by lymphocytic inflammation in nine of eleven (82%) samples that were relatively normal. In samples predominantly affected by reticulation ($\geq 50\%$ core volume, seven of 36), more severe fibrosis was observed at histopathologic analysis compared with samples with less reticulation (mean score, 1.6 vs 1.0; *P* = .04), accompanied by inflammation in all samples.

Severe ground-glass opacification ($\geq 40\%$ core volume, eight of 36) did not correlate with the grade of fibrosis (no fibrosis, *n* = 2; mild paraseptal fibrosis, *n* = 6). Inflammation was present in all but one sample with severe ground-glass opacification (seven of eight, 88%) while inflammation was present in 24 of the 28 (86%) samples without severe ground-glass opacification. Vasculopathy occurred independently of the presence or grade of fibrosis and was not associated with any of the radiologic estimations outlined herein.

Discussion

In the present study, we investigated the radiologic and histopathologic correlates of interstitial lung abnormalities (ILAs). We demonstrated that ground-glass opacification, reticulation, and bronchiectasis were the most frequent findings on ex vivo CT scans in lung specimens with ILAs. Paraseptal fibrosis (78% of samples) and accompanying (lymphocytic) inflammation (86% of samples) were most frequently observed at histopathologic assessment. In addition, we have demonstrated that the degree of fibrosis in relatively normal appearing lung regions with histopathologic evidence of moderate fibrosis (eight of 11 samples) and inflammation (nine of 11 samples) was underestimated at CT. The presence of reticulation on CT scans was associated with more extensive fibrosis at histopathologic assessment.

In our study, the most prominent findings in early-stage ILD included paraseptal fibrosis, lymphocytic inflammation, bronchiectasis, and some degree of vasculopathy, all of which are discussed in more detail as follows.

Paraseptal Fibrosis

Paraseptal fibrosis was most frequently observed in samples exhibiting fibrosis (28 of 30), indicating that fibrosis seems to originate from the periphery of the secondary pulmonary lobule, moving inwards to the interstitial and centrilobular areas. This was also observed in our previous study investigating radiologically normal-appearing areas in end-stage IPF lungs (9). We found that opacities in or near the interlobular septa were higher or enlarged, which causes reticulation and ultimately honeycombing as airway-like structures along the opacities enlarge and gradually fill the entire secondary pulmonary lobulus, giving rise to the typical honeycomb appearance that was not yet visible in our cohort with early ILD.

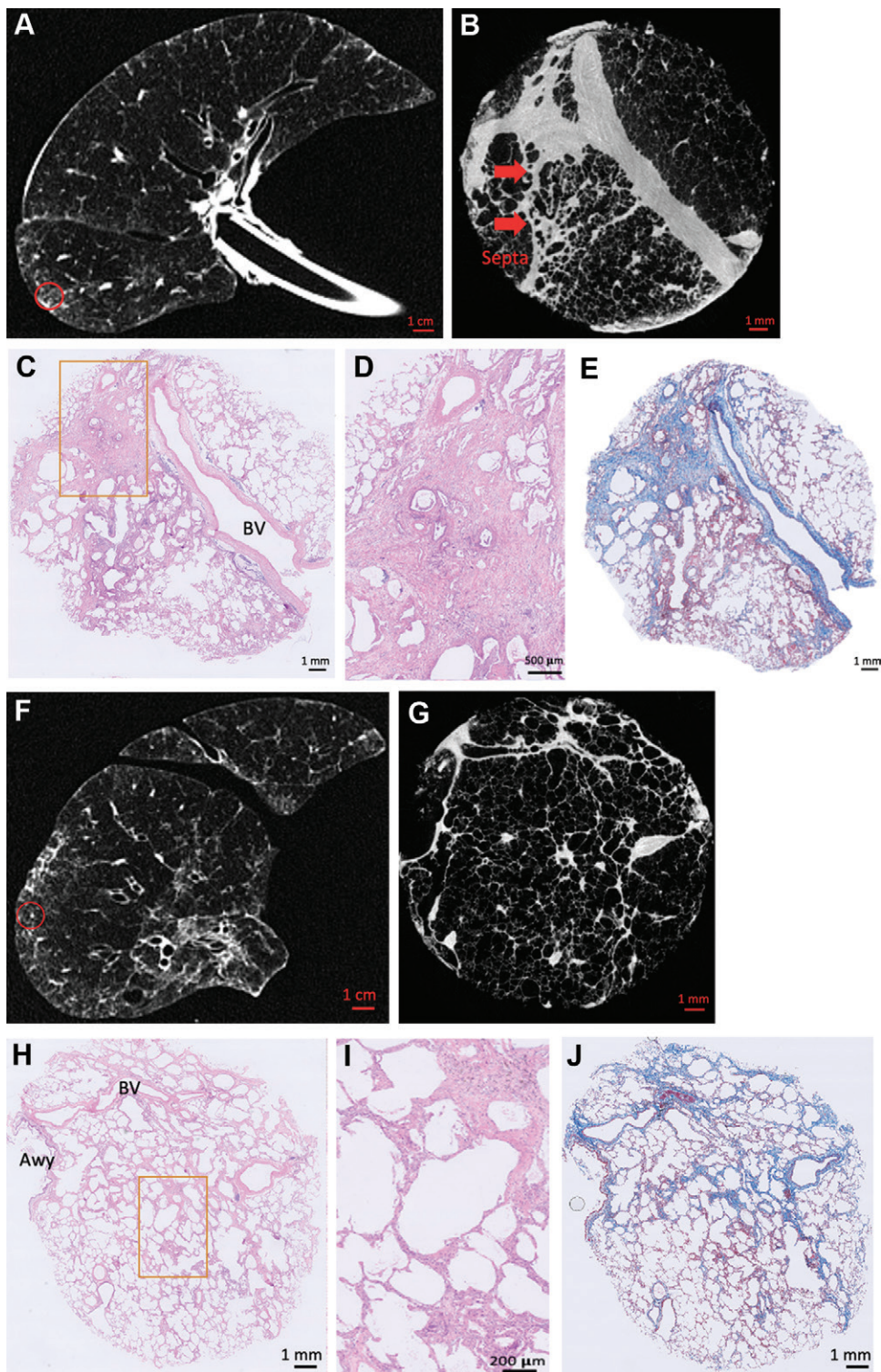


Figure 3: Illustrative examples of sampled lung areas with ex vivo CT, micro-CT, and histologic staining. **(A)** Axial noncontrast ex vivo CT scan shows highly abnormal (25% healthy, 55% reticulation, 20% ground-glass opacification) lung findings. **(B–E)** Micro-CT scan **(B)** and histopathologic images (hematoxylin-eosin **[C, D]** and trichrome **[E]** staining; magnification, $\times 5$ for **C** and **E**, $\times 20$ for **D**) of the area highlighted with the circle in **A** show paraseptal and interstitial fibrotic changes. **(F)** Axial noncontrast ex vivo CT scan shows lung considered healthy (80%), with mild ground-glass opacification (1.5%) and limited reticulation (5%). **(G–J)** Micro-CT scan **(G)** and histopathologic images (hematoxylin-eosin **[H, I]** and trichrome **[J]** staining; magnification, $\times 5$ for **H** and **J**, $\times 20$ for **I**) of the matched location (circle in **F**) show paraseptal and interstitial fibrosis. Awy = airway, BV = blood vessel.

Lymphocytic Inflammation

The role of inflammation in IPF genesis and progression remains controversial. Inflammation is believed to be induced by ongoing fibrosis, mostly due to the observation that anti-inflammatory trials were largely negative (11). Therefore, it is of interest that predominantly lymphocytic inflammation was found in a large proportion of the samples in our study and, moreover, inflammation was visible before the onset of true fibrosis. This agrees with a recent study by Luzina et al (12) that investigated the transcriptome of morphologically inconspicuous areas in IPF lungs and found a strong immune and inflammation-related signature, specifically of activated lymphocytes. However, this was only investigated in lungs with end-stage disease where the entire microenvironment is likely confounded by the universal presence of fibrotic remodeling in various stages and degrees, but where, nevertheless, different gene expression signatures are found in inconspicuous rather than fibrotic areas of parenchyma (13,14). The predominant pattern of fibrosis and inflammation also seem to go hand in hand, indicating their intriguing relationship. Our finding of lymphocytic inflammation in early disease may be of primary importance in ILD.

Bronchiectasis

We also observed radiologic evidence of bronchiectasis in five of eight specimens, while the corresponding histopathologic assessment demonstrated bronchiectasis in 14 of 36 samples and peribronchial fibrosis in 15 of 36 samples. Hida et al (15) demonstrated that 285 of 378 (75%) patients with ILAs showed some degree of bronchiectasis, which was associated with a worse outcome compared with patients with ILAs without bronchiectasis. Similarly, prognosis was worse in patients where bronchiectasis

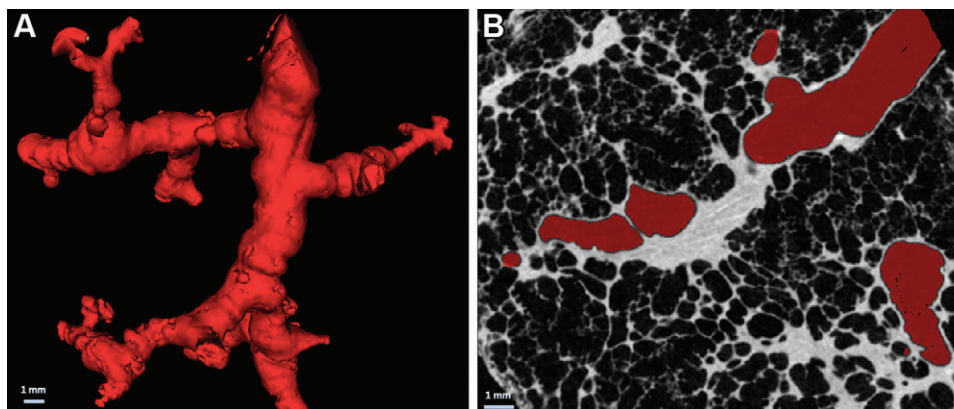


Figure 4: (A) Three-dimensional reconstruction of distal airway tree based on specimen micro-CT scans shows typical tortuous and distorted airways. (B) Cross-sectional micro-CT panel shows the absence of overt fibrosis in the vicinity of the airway, which is highlighted in red.

progressed over time (16). Consistently higher degrees of airway wall thickness have also been found in patients with ILAs and IPF (17), thereby supporting a pathophysiologic role of the airways in disease progression. This is in line with our own data indicating that small airways are decreased by 57% in lung explants with IPF, even in areas that are only minimally affected by fibrosis (6). The importance of the airways in IPF is further corroborated by biologic evidence that aberrant basal cells, the most important airway progenitor cell with the ability to proliferate and differentiate into virtually all epithelial cell types of the airway epithelium, have been found to be dysregulated in IPF (18). Our histopathologic assessment of ILA lungs also showed important peribronchial inflammation (25% of samples) and peribronchial fibrosis (42% of samples) in early disease specimens, further suggesting that the airways might play an important role in the pathophysiologic processes of IPF.

Vasculopathy

The role of the (micro) vasculature remains elusive in IPF/ILD. However, emerging data show an important role for vascular changes in the process of pulmonary fibrosis. Recent single-cell sequencing data identified a new type of vascular endothelial cell that might be involved in the progression of fibrosis in IPF (19). Along these lines, Ackermann et al (20) provided compelling evidence of increased intussusceptive angiogenesis, a rapid process of blood vessel neof ormation by splitting of a vessel into two lumens through incorporation of circulating angiogenic cells, in specific subtypes of ILD. Changes in the vessel-related structures, a computer-derived CT variable, is also a strong predictor of outcome in IPF (21).

By design and methodology, our study had limitations. Our specific comprehensive analytic approach precluded the analysis of many samples, and the availability of fresh whole lungs or lobes in such early stages of disease is limited. Prior studies included a matched control group revealing that substantial fibrosis can be observed in samples that show no radiologic abnormalities; no control group was available in our study. Due to the anonymity of the organ donation process, we do not have access to certain clinical variables, such as pulmonary function and

smoking status, or ethical permission to study genetic mutations (eg, *MUC5B* or telomere changes).

In conclusion, we have demonstrated that early histologic features of lung fibrosis, primarily encompassing paraseptal fibrosis, lymphocytic inflammation, and bronchiectasis, are present even in normal-appearing lung regions at CT. Future studies are required to further refine and validate the concept of interstitial lung abnormalities and their relation to the genesis and progression of interstitial lung disease.

Author contributions: Guarantors of integrity of entire study, S.E.V., W.A.W.; study concepts/study design or data acquisition or data analysis/interpretation, all authors; manuscript drafting or manuscript revision for important intellectual content, all authors; approval of final version of submitted manuscript, all authors; agrees to ensure any questions related to the work are appropriately resolved, all authors; literature research, S.E.V., J.J., T.G., J.H., L.J.C., G.M.V., J.V.; clinical studies, J.J., L.J.C., D.E.V.R., J.M.K.v.E., E.W., J.V.; experimental studies, A.V., L.D.S., A.P.N., M.N.B., D.D.J., J.V., W.A.W.; statistical analysis, S.E.V.; and manuscript editing, S.E.V., J.J., T.G., J.H., L.J.C., D.E.V.R., L.D.S., R.V., J.M.K.v.E., A.P.N., G.M.V., W.J., B.W., D.D.J., J.V.

Disclosures of conflicts of interest: S.E.V. Consulting fees from Boehringer Ingelheim, Sanofi, and Therakos; travel support paid to institution from GSK. A.V. No relevant relationships. J.J. Consulting fees and/or lecture payments from Boehringer Ingelheim, Roche, GlaxoSmithKline, NHXS, and Takeda; Patents planned, issued, or pending; advisory board, Boehringer Ingelheim and Roche. T.G. No relevant relationships. J.H. No relevant relationships. L.J.C. No relevant relationships. D.E.V.R. Supervisory board chair of Eurotransplant International Foundation; supported by the Broere Charitable Foundation. L.D.S. No relevant relationships. R.V. Advisory board, AstraZeneca and Takeda; chair, European Respiratory Society and European Cardio Thoracic Transplant Association. J.M.K.v.E. No relevant relationships. A.P.N. No relevant relationships. G.M.V. Advisory board, Zambon. M.N.B. Patents planned, issued, or pending. W.J. No relevant relationships. E.W. No relevant relationships. B.W. No relevant relationships. D.D.J. No relevant relationships. J.V. Lecture payment from Boehringer Ingelheim. W.A.W. Institutional grants and/or travel support and/or advisory board, Roche, Boehringer Ingelheim, and Galapagos.

References

1. Hatabu H, Hunninghake GM, Richeldi L, et al. Interstitial lung abnormalities detected incidentally on CT: a Position Paper from the Fleischner Society. *Lancet Respir Med* 2020;8(7):726–737.
2. Hunninghake GM. Interstitial lung abnormalities: erecting fences in the path towards advanced pulmonary fibrosis. *Thorax* 2019;74(5):506–511.
3. Miller ER, Putman RK, Vivero M, et al. Histopathology of Interstitial Lung Abnormalities in the Context of Lung Nodule Resections. *Am J Respir Crit Care Med* 2018;197(7):955–958.

4. Hung YP, Hunninghake GM, Miller ER, et al. Incidental nonneoplastic parenchymal findings in patients undergoing lung resection for mass lesions. *Hum Pathol* 2019;86:93–101.
5. Verleden SE, Vanstapel A, De Sadeleer L, et al. Quantitative analysis of airway obstruction in lymphangioleiomyomatosis. *Eur Respir J* 2020;56(1):1901965.
6. Verleden SE, Tanabe N, McDonough JE, et al. Small airways pathology in idiopathic pulmonary fibrosis: a retrospective cohort study. *Lancet Respir Med* 2020;8(6):573–584.
7. Verleden SE, Kirby M, Everaerts S, et al. Small airway loss in the physiologically ageing lung: a cross-sectional study in unused donor lungs. *Lancet Respir Med* 2021;9(2):167–174.
8. Verleden SE, Vanstapel A, De Sadeleer L, et al. Distinct Airway Involvement in Subtypes of End-Stage Fibrotic Pulmonary Sarcoidosis. *Chest* 2021;160(2):562–571.
9. Mai C, Verleden SE, McDonough JE, et al. Thin-Section CT Features of Idiopathic Pulmonary Fibrosis Correlated with Micro-CT and Histologic Analysis. *Radiology* 2017;283(1):252–263.
10. Masschaele B, Dierick M, Loo DV, et al. HECTOR: A 240kV micro-CT setup optimized for research. *J Phys Conf Ser* 2013;463:012012.
11. Heukels P, Moor CC, von der Thüsen JH, Wijsenbeek MS, Kool M. Inflammation and immunity in IPF pathogenesis and treatment. *Respir Med* 2019;147:79–91.
12. Luzina IG, Salcedo MV, Rojas-Peña ML, et al. Transcriptomic evidence of immune activation in macroscopically normal-appearing and scarred lung tissues in idiopathic pulmonary fibrosis. *Cell Immunol* 2018;325:1–13.
13. Jonigk D, Stark H, Braubach P, et al. Morphological and molecular motifs of fibrosing pulmonary injury patterns. *J Pathol Clin Res* 2019;5(4):256–271.
14. McDonough JE, Ahangari F, Li Q, et al. Transcriptional regulatory model of fibrosis progression in the human lung. *JCI Insight* 2019;4(22):e131597.
15. Hida T, Nishino M, Hino T, et al. Traction Bronchiectasis/Bronchiolectasis is Associated with Interstitial Lung Abnormality Mortality. *Eur J Radiol* 2020;129:109073.
16. Hino T, Hida T, Nishino M, et al. Progression of traction bronchiectasis/bronchiolectasis in interstitial lung abnormalities is associated with increased all-cause mortality: Age Gene/Environment Susceptibility-Reykjavik Study. *Eur J Radiol Open* 2021;8:100334.
17. Miller ER, Putman RK, Diaz AA, et al. Increased Airway Wall Thickness in Interstitial Lung Abnormalities and Idiopathic Pulmonary Fibrosis. *Ann Am Thorac Soc* 2019;16(4):447–454.
18. Carraro G, Mulay A, Yao C, et al. Single-Cell Reconstruction of Human Basal Cell Diversity in Normal and Idiopathic Pulmonary Fibrosis Lungs. *Am J Respir Crit Care Med* 2020;202(11):1540–1550.
19. Adams TS, Schupp JC, Poli S, et al. Single-cell RNA-seq reveals ectopic and aberrant lung-resident cell populations in idiopathic pulmonary fibrosis. *Sci Adv* 2020;6(28):eaba1983.
20. Ackermann M, Stark H, Neubert L, et al. Morphomolecular motifs of pulmonary neoangiogenesis in interstitial lung diseases. *Eur Respir J* 2020;55(3):1900933.
21. Jacob J, Bartholmai BJ, van Moersel CHM, et al. Longitudinal prediction of outcome in idiopathic pulmonary fibrosis using automated CT analysis. *Eur Respir J* 2019;54(3):1802341.
22. De Samber B, Renders, J, Elberfeld T, et al. FlexXCT: a Flexible X-ray CT scanner with 10 degrees of freedom. *Optics Express* 2021;29(3):3438–3457.